Highlights

Assessment of atmospheric and soil water stress impact on a tropical crop: the case of *Theobroma cacao* under Harmattan conditions in eastern Ghana.

Pietro Della Sala, Christian Cilas, Teresa E. Gimeno, Steven Wohl, Stephen Yaw Opoku, Alina Găinuşă-Bogdan, Fabienne Ribeyre

- Soil and atmospheric water stresses' effect on cacao's transpiration are independent

- Atmospheric stress reduced the canopy density by one third regardless of irrigation

- An extra third of the canopy density was lost due to soil water stress in the control

- Soil moisture and air vapour pressure are the key drivers of cacao sap velocity

- Cacao transpiration appears more limited by root uptake than canopy conductivity

Assessment of atmospheric and soil water stress impact on a tropical crop: the case of *Theobroma cacao* under Harmattan conditions in eastern Ghana.

Pietro Della Sala[a,b,*], Christian Cilas[b,c], Teresa E. Gimeno[e,f], Steven Wohl[e],
Stephen Yaw Opoku[d], Alina Găinușă-Bogdan[a], Fabienne Ribeyre[b]

[a]Rockwinds LBMS SAS, Bordeaux.
[b]CIRAD, UMR PHIM, 34090 Montpellier, France
PHIM Plant Health Institute, Univ Montpellier, CIRAD, INRAE, Institut Agro, IRD,
Montpellier, France
[c]CIRAD, DGDRS, Abidjan, Côte d'Ivoire.
[d]Cocoa Research Institute of Ghana, New Tafo Akyem, Eastern Region Ghana. P.O 8.
[e]Basque Centre for Climate Change (BC3), 48940, Leioa, Spain.
[f]IKERBASQUE, Basque Foundation for Science, 48008, Bilbao, Spain.

Abstract

In West Africa, Harmattan-induced atmospheric and soil droughts represent seasonally recurring hazards for *Theobroma cacao* L. agro-ecosystems. Under the influence of the Harmattan winds, precipitation is impaired and air humidity and temperature reach stressful levels. Climate change is causing an increase in temperature that will drive up the evaporative power of the atmosphere, risking to harshen both the soil and atmospheric stress. This would further threaten the viability of cacao cultivation in this region. To characterize the response of cacao trees to atmospheric and soil drought, we monitored two sub-plots, with and without irrigation, throughout one Harmattan season (November 2019 - March 2020) in the Eastern region in Ghana. For both treatments we recorded: sap flow velocity, photosynthetic active radiation (PAR) above and below the canopy, soil moisture, temperature, air humidity and daily precipitation. Leaf area index (LAI) was estimated from PAR measurements. To characterize drought responses of mature cocoa trees during the day and at the seasonal scale, we developed two boosted regression trees models (BRT)

*[*]p.dellasala@rockwinds.com (Pietro Della Sala)

with the environmental variables measured. The atmospheric component of Harmattan-induced drought was found to affect the canopy to a similar extent as soil water stress, both causing a decline in LAI of 33%. This study confirmed the importance of soil drought but highlighted as well the crucial role of atmospheric drought for this species' transpiration control. Soil and atmospheric water stresses did not have a synergistic effect on transpiration under the studied conditions. The BRT models identified LAI as one of the most influential drivers for sap velocity, which, in turn was sensitive to the interactive effect of both atmospheric and soil drought. Our results highlight that not only reduced precipitation but also increasing atmospheric drought is likely to negatively impact on cacao production in West Africa under increasingly dry conditions imposed by the influence of the Harmattan winds.

2

1. Introduction

The global climate has changed over the past century and is projected to continue to change in the next decades at a higher pace than in the past [1]. Global general circulation models (GCMs) agree that, except for an unlikely low emissions scenario, by the end of this century, global mean temperatures will rise by at least another 1.5°C and precipitation regimes over large areas worldwide will experience profound changes. In the tropical band (23°3'N-23°3'S), climate change is expected to have a negative impact on agriculture, ultimately threatening the economic stability of countries that rely heavily on this sector. This is particularly true for West Africa where agricultural systems are among the most vulnerable worldwide due to the economic constraints limiting access to agricultural technological advances, among other reasons [2, 3, 4]. West Africa's most famous exported crop, cacao (*Theobroma cacao* L.), will experience a severe reduction of its agro-pedo-climatic zone of cultivation [5, 6, 7]. Recent model predictions based on the SRES-A2 greenhouse gas emission scenario [8] project a continued rise in mean temperatures over the West African cocoa belt in the future and, while cumulative annual precipitations are not expected to change significantly, their distribution over the course of the year is. The period with no precipitations whatsoever may slightly shorten or remain unchanged in the coming decades across West Africa but, due to the aforementioned increase in temperatures, this region is expected to experience longer periods under greater evaporative demand. Ultimately, this will result into increased frequency, severity and duration of episodes of both soil and atmospheric water stress at the plant level. Consequently, a large share of cocoa-producing regions in West Africa will become unsuitable for production in the future [5, 6, 7], leaving millions of smallholder farmers without a reliable source of income [9].
The West African long dry season is characterized by the co-occurrence of low precipitation and a dry wind, the Harmattan. The Harmattan is a north-easterly trade wind blowing over North Africa that results from the continental-scale pressure gradient between the subtropical subsidence zone and the Intertropical

3

Convergence Zone (ITCZ) [10]. During the West African dry season, corresponding to the boreal winter, the Harmattan advances to the southern part of West Africa conveying a dry air mass from the Sahara to the south which lingers around the northern edge of the cacao belt, along the Gulf of Guinea [10]. The presence of the Harmattan hinders moist convection and suppresses any chance of precipitations, only allowing for sporadic weak rains for hundreds of kilometers south of the Intertropical Front, that marks the southern Harmattan extent at ground level [11]. The Harmattan further enhances soil and air water stress as the evaporative demand increases due to higher wind speed and reduced air humidity, ultimately leading to wide temperature differentials from day to night. Hence, under the influence of the Harmattan, soil water content decreases due to the lack of precipitation together with increased evaporative demand at the leaf level.

Cacao is original from the Amazon basin, where water limitation is virtually inexistent [12, 13, 14]. The morphological traits of cacao are not adapted to deal with water limitation: for example, cacao has large, broad leaves with minimal waxing and high stomatal density that cause strong transpiration and evaporation rates under high irradiance or high vapor pressure deficit (VPD) [15]. The hydraulic system of cacao is also poorly adapted to low water availability: the main stem has wide xylem vessels [16] to pump water more efficiently from the soil to the leaves, but this implies a greater risk of functionality loss due to cavitation under water stress [17]. Moreover, the cacao root system is relatively shallow, with high density of fine roots in the top 0.2-0.6 m of the soil, and hence it cannot access deep water [18, 19]. The physiological performance of cacao is also adapted to its native climatic conditions. Cacao optimum growth temperature is 24°C at night and 30°C during the day [20]. Cacao photosynthetic efficiency starts declining at temperatures above 33°C, while night temperatures below 15.8°C suffice to observe a decline in photosynthesis and stomatal conductance [17]. Additionally, for cacao trees of the Amelonado family, genetically the most representative in West Africa, the reported base temperature for vegetative growth is 19.7°C [21]. In West Africa, during the dry season and

4

under the influence of the Harmattan, air humidity is not sufficient to buffer large daily thermal oscillations and air temperature can reach values as high as 44°C [22, 23] and as low as 12-14°C at night [24, 25]. These large daily temperature oscillations strongly inhibit the net growth and physiological performance of cacao [20]. In addition, reduced air humidity due to the influence of the Harmattan has a direct, negative effect on growth and physiological performance. Indeed, in tropical environments it has been shown that 60% is the air humidity threshold below which tree physiological performance starts to decrease and below 40%, in combination with high temperatures, it is considered that trees are exposed to high atmospheric water stress [26, 27]. It can be assumed that such conditions would be stressful for cacao as well, in line with [28]. Overall, it is clear that cacao lacks high tolerance to drought or extreme temperatures. Thus, the viability of cultivation of this crop outside its native range, in West Africa, is severely threatened by future climate change. The future threats to cacao cultivation are further exacerbated in full sun or lightly shaded monocoltural systems, preferred by farmers across West Africa for the higher yields in the short term but more exposed to atmospheric stress [23].

Both soil and atmospheric drought impact negatively on plant growth and productivity [29, 30]. Plants first respond to increasing vapour pressure deficit (VPD) by closing their pores on their leaf surfaces, the stomata, to reduce transpiration water loss, but this also entails a reduction in CO_2 uptake to supply photosynthesis and, eventually, reduced growth and production of reproductive structures [31, 32]. On the other hand, soil drought reduces the conductivity of the soil-plant-atmosphere continuum, ultimately inducing stomatal closure to protect the hydraulic system of the plant from embolism [33, 34]. Beyond stomatal closure, high VPD also increases non-stomatal water losses, for example through the cuticle, further increasing risk of hydraulic failure [14, 16, 35]. Besides reducing photosynthesis, soil drought also reduces xylem and phloem transport and, hence, export of carbohydrates from the leaves to reproductive organs for flower and fruit production [36, 30].

Several authors have already highlighted the need to better investigate the water

5

relations of cacao under field conditions [37], but we still lack a detailed characterization of how drought stress influences cacao physiology and reproduction [17]. The effects of relative humidity [28] and temperature have been addressed [20, 38, 21] and a few field trials have addressed soil drought stress but, to our knowledge, no previous study has assessed the simultaneous effect of soil and atmospheric drought, and their interaction [18, 19, 23]. The reduction of transpiration in response to soil water stress has been characterized in Brazil [13] and Indonesia [18, 19], but in these locations VPD and air temperature rarely reach stressful conditions for the trees. Such effects have not been addressed in the West African cacao belt, where radically different atmospheric conditions due to the influence of the Harmattan will likely impose drought stress levels beyond those previously studied. The objective of this study is to clarify the effects of atmospheric and soil water stress on cacao tree transpiration during the dry Harmattan season and shed light on the drivers of transpiration under such circumstances. Our hypothesis is that cacao trees will respond strongly to both types of stresses but we expect VPD to be more influential, due to the extremely low relative humidities and large temperature oscillations experienced under the influence of the Harmattan.
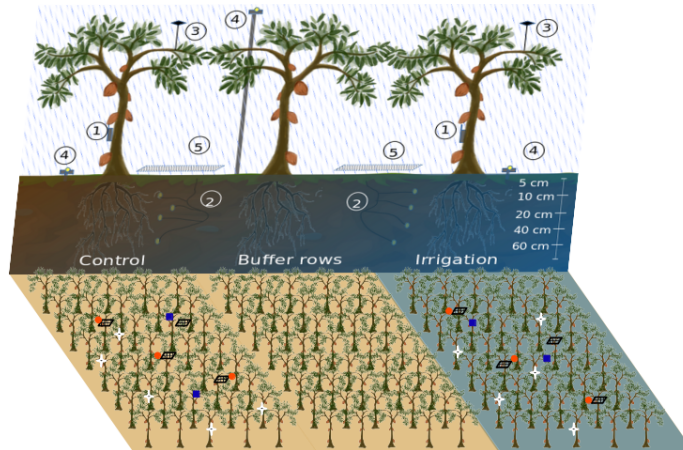
2. Materials and methods

Figure 1: Schematic representation of the field experimental plan with an overview of the measurements taken. The experiment compared an irrigated plot (5 rows of 8 trees) to a control rain-fed one. The experimental plots were separated by a buffer of ten rows of trees. In each plot we measured 1) sap velocity (crosses), 2) soil moisture (squares), 3) temperature and air relative humidity, 4) photosynthetically active radiation (PAR) above and below the canopy (dots) and 5) litterfall production (hatched parallelograms). Position of the sensors reflect their real position in the field experiment. Graphics by Pietro Della Sala, drawing of the cacao tree by Estelle Ribeyre.

2.1. Study site and experimental design

Two plots of cacao trees, with and without irrigation, were monitored throughout the duration of the experiment (3rd December 2019 to 16th March 2020) and their response to climate tracked closely by means of various sensors. The measured environmental variables were: soil volumetric water content at four depths from 10 to 60 cm, air temperature, air relative humidity and photosynthetically active radiation (Fig. 1).

The study was conducted at the experimental station of the Cacao Research Institute of Ghana (CRIG) located in New Tafo Akyem, Eastern Region, Ghana (6°13'53.7"N; 0°21'01.6"W; 203 m a.s.l.). At this location, the climate is warm and humid all year round except for two dry seasons. The main dry season has

7

its core between December and February, but the onset can be as early as mid November and lasts until sometime in March. The second dry season occurs between the second half of July and the beginning of September and is typically much less severe than the main dry season.

Throughout the year, temperature in Tafo oscillates between a monthly average minimum of 20 to 22°C and a monthly average maximum of 29 to 33°C [39]. Annual rainfall ranges between 1150 and 1800 mm with a mean value of 1565 mm per year [39, 40].

At the study site, a 2 ha cacao plantation was established in June 2013. Cacao trees (*Theobroma cacao* L.), of homogeneous genetic origin, were planted with a 2.5 x 2.5 m spacing (1600 trees ha^{-1}), underneath *Gliricidia sepium* Jacq. previously planted at a density of 10 trees ha^{-1}. The plantation consisted of four blocks with 10 plots each. Each plot contained 40 trees planted in five rows with eight trees per row. In November 2019, two plots of 40 hybrid Amelonado trees with mean canopy height of 3 meters were selected for the study. The selected plots were located at least 20 m away from the nearest shading tree and, therefore, were considered as a "typical West African full sun system". The two study plots were separated by ten rows of cacao trees to avoid any edge effect or interaction between the two (Fig. 1). From the 26th of November 2019 to the 16th of March 2020, trees in one plot (irrigation treatment) were irrigated with 60 L per tree (equivalent to approximately 9.6 mm per tree) on alternating dates using a hose, whereas trees in the second plot (control) only received ambient precipitation. The irrigation was evenly applied within 50 cm from the trunk, where most of the roots were believed to be distributed [37]. Irrigation close to the trunk was not reduced by losses due to canopy interception, thus its efficacy was higher than a rainfall of 9.6 mm.

2.2. Soil properties

According to a soil analysis of the experimental site conducted in March 2020, the upper soil (0-15 cm) was a eutric fluvisol with sandy-loam texture and below 15 cm of depth the soil texture was sandy clay loam. The pH was 6.5

across the entire profile. The upper soil was poor: organic matter content was 1.36%, magnesium was 2.06 $me*100g^{-1}$, total nitrogen was 0.15 %, ammonium was 14.2 ppm, phosphorus was 12.96 ppm, potassium was 0.049 $me*100g^{-1}$ and exchangeable calcium was 3.72 $me*100g^{-1}$. Based on the soil texture at a depth of 30 cm, the bulk density (BD), field capacity (FC) and permanent wilting point (PWP) were estimated in 1.45 $g*cm^{-3}$, 34% and 13%, respectively. Below 30 cm, the values of BD, FC and PWP were 1.55 $g*cm^{-3}$, 35 and 16%, respectively.

2.3. Transpiration measurements

For the entire duration of the experiment, tree transpiration was estimated from measurements of sap velocity using the Heat Ratio Method (HRM: [41]). Five trees in each plot were selected, with mean±sd diameters (measured 20 cm below the main branch) of 11.31±1.84 and 12.23±1.34 cm in the control and irrigated plots, respectively (Fig. 1, (1)). Within each plot, the trees were selected based on a visual scoring system of overall condition (canopy density, leaf greenness, number and diameter of jorquette branches etc.) and avoiding spatial clustering of monitored trees. In November 2019, we installed one heat probe sensor (SF-3, East30sensors, USA) on each selected tree. Each sensor consisted of three probes, 35 mm in length, 1.3 mm in diameter, and 6 mm axial distance apart. The central probe contained an evanohm heater, and the lateral two probes, one upstream and one downstream with respect to the heater, contained 3 thermistors placed at 5 mm, 17.5 mm, and 30 mm from the sensor tip to monitor sap flow across the entire depth of the sapwood. The thermistor temperature sensor consisted of a 10K precision resistor and a 10K thermistor wired through a three wire half bridge connected to a datalogger per irrigation treatment (CR800, Campbell Scientific, Logan, UT, USA). The accuracy of the thermistors was ±0.2 °C, and the resolution was 0.001 °C. The central needle was heated by a 12V pulse of 3 seconds powered by the datalogger and reduced to 5V through a heat control board (East30sensors, USA).

Sensors were installed on the trunk following the xylem direction, at a minimum

distance of 20 cm from any node or branching and at a minimum height from the soil of 50 cm. Bark thickness was 0.3±0.15 cm (n = 10 trees) and was kept in place to protect the wound from dryness and fungal attacks. The probes were programmed in accordance with the Dual Method Approach (DMA: [42]). The DMA combines the traditional approach to calculate sap velocity from heat pulse velocity [41] with the Tmax Method [43]. The latter allows to capture high and low flow rates both upward and downward along the stem [42]. Three values of heat pulse velocity were recorded every 30 minutes per sensor. Each value was calculated from the temperature difference between each pair of up- and down-flow thermistors located at three depths within the sapwood (5, 17.5 and 30 mm from the bark). Sap velocity was calculated for each of the three positions and then upscaled to an integrated value of sap flux for each tree through a weighted sum based on the sapwood area, estimated through wood coring, associated to the specific radial position [42]. Before upscaling to a single value per tree, each couples of thermocouples was calibrated to have the zero for sap velocity when night potential evapotranspiration was zero (S. 2.6) [44, 45]. In this study it was assumed that during the three months of dry season the sapwood area increment is negligible, therefore, changes in transpiration are approximated to variations in sap flux.

2.4. Soil VWC

Soil volumetric water content (VWC) was monitored in two flat locations per plot, equidistant (170 cm) to all surrounding trees, at four depths (10, 20, 40, and 60 cm), with TEROS 10 capacitance probes (METER group, Pullman,WA, USA) (Fig. 1, (2)). The chosen distance allowed to capture the average VWC of both the irrigated and the non-irrigated plots, avoiding potential biases due to uneven irrigation in the former. Despite their distance from the trees, the locations for VWC monitoring were shaded by the plots' closed canopy, effectively limiting quick evaporation of water after a watering event, be it rainfall or irrigation. The TEROS 10 sensors estimate soil VWC from measurements of the apparent dielectric permittivity in the 430 mL of surrounding medium. For

this study, the manufacturer's calibration for a generic mineral soil was used. A value of soil VWC per probe was recorded on a CR800 datalogger every 30 minutes from November 26th 2019 to March 16th 2020. In one instance, the soil VWC was transformed into water potential to compare our results with other reported results. To obtain the pedotransfer function it was adopted the model by Van Genuchten [46]. The parametrization of the model was done with the R package *soilphysics 4.0* [47] and the soil properties measured with the soil analysis.

2.5. Leaf area index

Leaf Area Index (LAI) was estimated from measurements of photosynthetically active radiation (PAR) above (I) and below (I_0) the canopy (Fig. 1, (4)) in an inverted form of Beer's law (Eq. (1)). Measurements of PAR were collected from November 26th 2019 to March 16th 2020, with a brief interruption from December 27th 2019 to January 8th 2020. Incoming photosynthetic active radiation (PAR; $\mu mol * s^{-1} * m^{-2}$) above the canopy was measured every 30 minutes at one position in the irrigated plot. The PAR sensor (SQ110, Apogee instruments, Santa Monica, CA, USA) was mounted on top of a 5 m levelled iron pipe planted in the soil, i.e., 2 m above the canopy. Additionally, PAR was monitored under the canopy at three locations in each plot with three sensors mounted on levelled poles at 20 cm height. The extinction coefficient (K), necessary to calculate LAI from PAR data (Eq. (1)), depends on the solar angle (ϕ) and a leaf angle distribution coefficient (x) and was calculated applying Eq. (2) [48]. The parameter x was calculated as the ratio of vertical to horizontal projections of the canopy [48]. Based on field measurements, x was evaluated at 1.2, corresponding to an ellipsoid leaf angle distribution. A reliable estimation of K is possible only when the solar angle is close to the zenith [49, 50], therefore, we estimated LAI from PAR measurements collected between 10:30 and 14:30 (solar time). Furthermore, to avoid overestimation of LAI due to excess direct radiation reaching the sensors under the canopy, data from each sensor were smoothed and interpolated with the *Daniell* modified Fourier method [51, 52]

and the three resulting curves averaged to get a final LAI value for the entire plot.

$$\frac{I}{I_0} = e^{-K*LAI} \tag{1}$$

$$K = \frac{\sqrt{x^2 + 1/tan^2\phi}}{1.47 + 0.45x + 0.1223x^2 - 0.013x^3 + 0.000509x^4} \tag{2}$$

LAI change due to defoliation was also monitored through the same monitoring period with a set of four litter traps per treatment (Fig. 1, (5)). Each trap consisted on a suspended fine net of 1.2 m^2 that was positioned in randomized locations within each plot. The litter production was collected every 15 days and oven-dried at 100 °C for 36 hours to obtain the dry weight. To convert the leaf dry weight in LAI, in the beginning of the experiment the mean specific leaf area (SLA $cm^2 * g[dryleaf]^{-1}$) was calculated. A sample of 30 leaves (10 from the lower, middle and top canopy) for each treatment plot was scanned on a reference surface (an A4 sheet). The total area was estimated as the percentage of the images that was not white with ImageJ 1.53a [53]. To obtain the SLA, the average leaf area was divided by its oven-dry weight.

2.6. Atmospheric conditions

Air temperature and relative humidity were logged hourly in each plot, with with two iButtons (DS1923-F5: Hygrochron, iButtonLink LLC, Whitewater, WI,USA) above the canopy at c.a. 5 m height. To protect the sensors from direct radiation and precipitation, these were installed facing the ground, glued to the internal part of bottle caps (Fig. 1, (3)). As temperature and relative humidity were logged hourly and as they represent continuous variables, a linear interpolation was applied in order to obtain half-hourly time series that matched those of the other measured variables in the data set. The vapour pressure deficit (VPD) and night-time potential evapotranspiration (required to calibrate the zero for sap velocity) were calculated following the FAO-56 Penman-Monteith method [54] by means of the Python package *'opencroplib==0.1.5'* [55]. For the calculation of the night-time potential evapotranspiration was considered a

wind velocity above the canopy of 0.77 $m * s^{-1}$ at 5 m, in compliance with the average night-time value from a weather station at less than 1 km from the site. Daily precipitation data between October 1st, 2019 and March 16th, 2020 were retrieved from the Unified Gauge-Based Analysis of Daily Precipitation of the NOAA Climate Prediction Center (CPC; [40]).

2.7. Statistical analysis

Prior to analysis, we checked for sensor glitches, numerical artefacts of the sensor raw signal and measurement errors caused by faulty sensors. All measured variables but sap velocity were treated as continuous, with the hypothesis that they cannot abruptly change over half an hour. For this reason, it was decided to study the evolution of their first derivative in time and consider as outliers the points whose absolute value lied outside the two standard deviations confidence interval. A graphical evaluation of the data points flagged as outliers was carried out before they were discarded.

2.7.1. GAMM analysis

A generalized additive mixed model (GAMM) was used to model and assess the differences between the irrigated and non-irrigated plot dynamics of LAI over time. The GAM family of models was chosen primary because LAI was expected to exhibit a complex non-linear relationship with the environment. Secondly, it was necessary to use a GAMM because LAI measures in time were not completely independent as they were taken from the same sensors. Lastly, the choice to use a GAMM was dictated by the fact that for each date we had only few points for LAI, thus large variance. It would have been difficult to appreciate the difference without the GAMM model capturing the time evolution of LAI. The built GAMM model fitted a gaussian distribution for LAI (continuous variable) using the treatment (irrigated or control) as fixed effects and taking into account the random sensor-to-sensor variability. The effect of time was fitted by a smooth term using Duchon splines, allowing the the predictions to take into account the differential in water availability due to

13

irrigation. The GAMM-modeled LAI for both watering treatments was plotted and we interpreted non-overlapping 95% confidence intervals as a significant difference between treatment levels for a given period. All these analyses were performed in the R environment v3.6.1 [56] using packages plyr [57], tidyverse v1.3.0 [58], mgcv [59] and itsadug v2.3 [60].

2.7.2. Boosted Regression Tree analysis

We used Boosted Regression Trees analysis (BRT) modelling to predict transpiration from climatic variables [61]. BRT uses two algorithms: regression tree and boosting. Tree-based regression models, described for use in ecology by [62], partition the solutions space with a set of rules, identifying the most homogeneous regions in terms of response to predictors. They then fit a constant to each region, fitting the average response in that region with the assumption of normally distributed errors. With each iteration the tree grows by repeatedly applying the analysis of the predictors space to its own output until a user-defined stopping criterion is reached. Tree-based models are intuitive, easy to visualize and are fairly insensitive to outliers, missing data and data types (numeric, binary, categorical etc.) but they lack the accuracy of other methods, such as GLM and GAMM. To compensate for this downside it is convenient to combine tree-based models with boosting. The idea behind the boosting methods is that it is more probable to find many rules of thumb, than to find a single, highly accurate prediction rule [63]. It is, therefore, more convenient to approximate the solution by averaging the results of a large number of rules of thumb rather than aiming for a unique highly accurate one. The BRT uses boosting as a way to evaluate the gradient of the predictors space by focusing on the variation in the response not explained yet by the model at a given step and fitting a new tree to its residuals [64]. Through boosting, decision trees are fitted iteratively to the training data, increasingly emphasising the still poorly modelled observations. As the boosting process is stage-wise, existing trees are left unchanged as the model is enlarged but the fitted value is estimated at each step to reflect the contribution of the newly added tree. The final BRT model

14

328 is a linear regression model where each term is a tree.

329 In order to ensure the stability of the models' results and avert over-fitting,
330 the evaluation looked at the difference between the training data coefficient of
331 correlation and the coefficient of correlation for the 100-fold cross-validation.
332 The skill of the models, instead, was assessed by plotting the predicted values
333 against the measured ones [61, 64].

334 The BRT analyses were carried out using R v3.6.1 [56] and the gbm [65] and
335 dismo [66] packages. The parameterization of the two models can be found in
336 Tab. C.3.

337 Two BRT models were built using 75% of the dataset to explain the relative
338 importance of the potential drivers of transpiration during the dry Harmattan
339 season. The remaining 25% was used to fit the models and evaluate them
340 against the measured values. The two BRT models considered soil volumetric
341 water content (VWC), photosynthetic active radiation above the canopy (PAR)
342 and the vapour pressure deficit of the atmosphere (VPD) as environmental
343 predictors, the leaf area index (LAI) of the two plots as indicator of the general
344 state of the canopy and the diameter of individual trees as a proxy for their
345 dimension. The first model (model 1) used the half-hourly daytime data (PAR
346 $> 15 \ \mu mol * s^{-1} * m^{-2}$) to investigate the importance of each aforementioned
347 predictors in determining the daily daytime cycle of sap velocity. The second
348 model (model 2) investigated the role of the same predictors at the time scale
349 of one day; for this, the input variables as well as sap velocity were averaged
350 over the period of the day with a PAR above 15 $\mu mol * s^{-1} * m^{-2}$.

351 To avoid possible co-variations due to a common daily cycle, for the first
352 model it was decided to remove the daily pattern from the vapor pressure deficit
353 and radiation, maintaining only the effects due to the variation from the average
354 daily cycle. The global daily pattern was maintained as a separate variable, i.e.,
355 the hour of the day (Hour), and included among the predictors.

356 The two models were based on the assumption of a normal distribution of the
357 data (family = "Gaussian") and parameterized to avoid over-fitting (Tab. C.3)
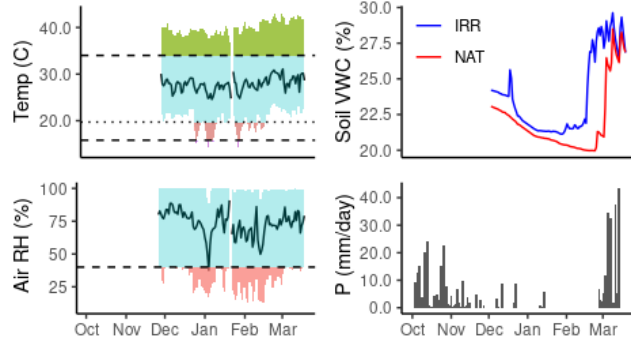358 [61, 64].

15

3. Results

3.1. Climatic conditions

Figure 2: Climatic conditions during the study period. Left top: mean daily air temperature (solid black line), the thresholds for photosynthetic decline (34 and 15.8°C) and observed base temperature for vegetative growth (19.7°C) [17] (dashed lines) and the range of values (shaded area) are depicted. Left bottom: mean daily relative air humidity (solid black line) with the threshold of 40% (dashed line) and its range of observed values (shaded area). Right top: average soil VWC for the entire profile (10 to 60 cm) for the irrigated (blue line) and non irrigated (red line) plots. Right bottom: daily precipitation.

The average daily temperature during the experiment (26th of November, 2019 -18th of March, 2020) was 27.8 ± 1.5 °C, and the maximum and minimum recorded temperatures were 43.1 °C and 13.6 °C respectively (Fig. 2). Between January and February, the site experienced the hottest temperatures and the largest daily thermal oscillations, surpassing both the upper and lower thresholds for maintaining photosynthesis for several hours. Temperatures above the threshold at which photosynthesis declines (34 °C), were recorded throughout the entire period under analysis on average for 6.5 ± 1.5 hours a day (Fig. A.1). Temperatures below the lower threshold for photosynthetic efficiency (19.7 °C), instead, occurred only in January and February when the Harmattan winds reached the site. Relative humidity fell below 40% for the first time in early December and, from late December until March, the site experience several hours with RH below 40% almost daily (Fig. A.1), reaching up to fifteen hours per

16

day below 40% in January. During our study period, the total precipitation was 116 mm, of which 92 mm fell in March while the remaining 24 mm were distributed in sporadic events from December to February. Prior to the onset of our study, in October and November 2019, the site received 222 mm of precipitation. The average soil VWC across the entire 10 - 60 cm profile was always higher in the irrigated treatment than in the control throughout the experiment. Soil VWC was above 21% in January and February in the irrigated plot, while in the non-irrigated (control) plot, VWC continued to decline below 20% over the same period. VWC quickly recovered in both treatments in March, when rains resumed.
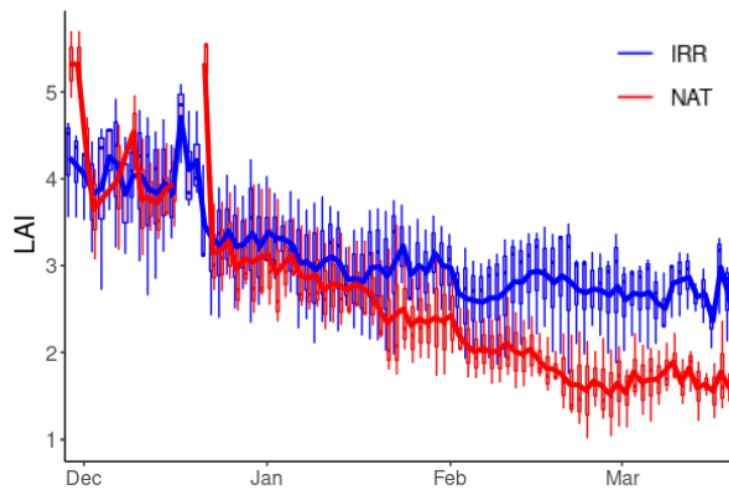
3.2. Leaf area index (LAI)

Figure 3: Leaf area index (LAI: $m^2[leaf] * m^{-2}[soil]$) in the two watering treatments: irrigated (blue) and control (red), throughout the observed dry season. The lines represent the three day-moving averages of the LAI times series. Box-plots represent the variability between the three sensors in each plot for every date.

Overall, LAI declined steadily throughout the experiment both in the irrigated and in the control plot. Throughout December, the LAI remained constant and started to decrease in January, in both treatment plots, at the same

17

time as the number of days with RH < 40% started to increase (Fig. 3, Fig. A.1). In February, LAI continued to decrease, faster in the non-irrigated (control) plot than in the irrigated one. At the end of the study, the estimated LAI was 2.7 $m^2[leaf] * m^{-2}[soil]$ at the irrigated plot and 1.5 $m^2[leaf] * m^{-2}[soil]$ at the non-irrigated plot compared to an estimated 4 $m^2[leaf] * m^{-2}[soil]$ in the beginning of the study for both treatments (Fig. 3). The LAI, thus, dropped by approximately 32.5% in the irrigated plot and by approximately 62.5% in the control. According to the GAMM, from mid-February onwards, LAI in the irrigated plot was significantly higher than in the control plot (Fig. B.1).

The total litter collected throughout the entire experiment was greater in the control (309 $g[dry] * m^{-2}$) than in the irrigated (247 $g[dry] * m^{-2}$) treatment. Most of the shedding appears to have occurred in late December for both treatments, while in March, with the resumption of rain, the litterfall went to zero (Fig. B.2). The average litterfall was lower in the irrigated plot, notably in the first week of January (Fig. B.2), when air humidity dropped below 40% for the first time. (Fig. 2). This is in agreement with the results of LAI dynamic that evidenced a difference in LAI between plots at the end of the season resulting from a steadily larger foliage loss in the non-irrigated plot (Fig. 3, Fig. B.2).

3.3. Sub-daily patterns of sap velocity in response to climatic drivers

Figure 4 shows the response of sap velocity to VPD under different levels of PAR above the canopy in the two treatments. At low VPD values (<1 kPa) trees in the control plot seem to have transpired more than those in the irrigated plot. Under high VPD (> 4 kPa), measurements of sap flow velocity from trees from both treatments presented a high dispersion regardless of the PAR level. Under intermediate VPD (2-4 kPa), sap velocity appeared to respond more to PAR in trees from the irrigated plot. ~~In Figure 5 is reported~~ Figure 5 shows the average daily cycle of sap velocity during the 25% most and least stressing days over the study period. Sap velocity at low VPD followed the same cycle in the two plots without significant differences except in the early morning when
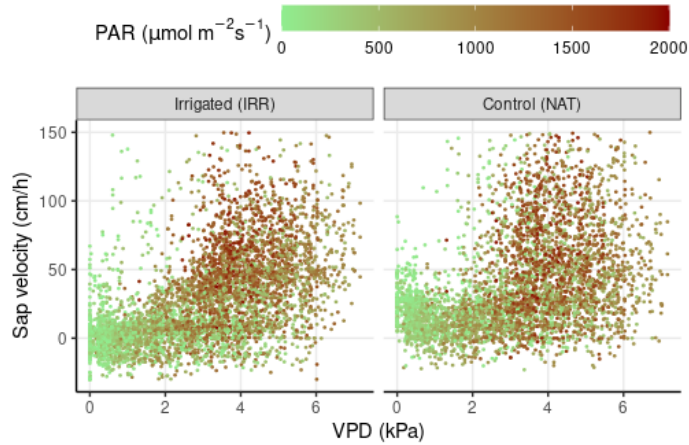
Figure 4: Sub-daily daytime measurements of cacao trees sap velocity in response to varying VPD: in the irrigated plot (left) and in the control plot (right) during the dry Harmattan season. Symbol colours depict PAR levels measured above the canopy (in $\mu mol * s^{-1} * m^{-2}$).

the control trees transpired significantly more than the irrigated ones (Fig. 5 B). Although, at low VPD the control trees presented a tendency to reach a higher midday sap velocity and have higher sap velocity. It is reported as a tendency because the confidence interval of the two curves overlaps (Fig. 5 B). In days when VPD was high the average sap velocity peaked around 70 cm/h for both treatments but the irrigated plot presented on average a sap velocity higher than the control during the late mornings while the control tended to maintain a higher sap velocity in the late afternoon (Fig. 5 A). In the morning the control presented a peak in sap velocity around 6 a.m. (20 cm/h), regardless of the level of VPD. A similar phenomenon was An early morning peak in sap velocity was also found for the irrigated plot in days when VPD was high. Both Figure 4 and 5 hinted to some behaviours that were not always easy to grasp, thus the importance of the study with the two BRT models.

The main drivers of half-hourly variations in sap velocity during the day were identified by means of a BRT model (model 1) (Figure Fig. 6). The model averted over-fitting and was considered to be stable (training data correlation = 0.885; cross-validation correlation coefficient = 0.741). A regression analysis of
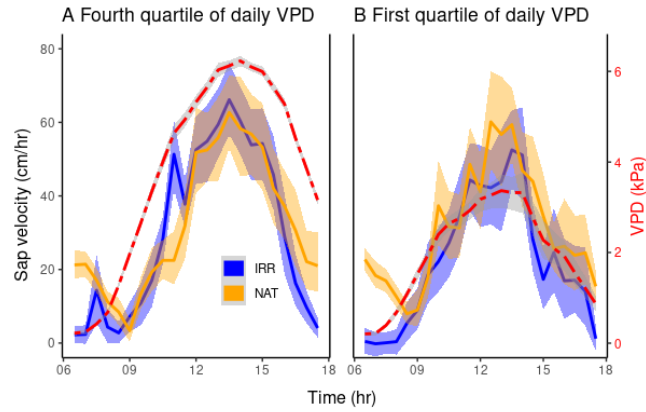
Figure 5: Sap velocity average daily cycle for cacao trees under high (A) and low (B) VPD conditions. The dashed line represents the average VPD cycle. The average cycles for sap velocity and VPD were obtained using the data from the 25% most and least stressing days of the dry Harmattan season 2019/2020. The shadings depict the the 95% confidence interval.
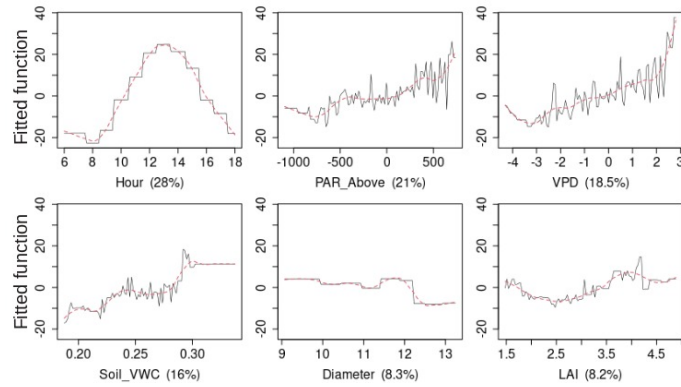

Figure 6: Overview of daytime sap velocity response to the main environmental drivers as identified with a BRT model (model 1). The responses are calculated on half-hourly data during the entire period of this study. Functional shapes of the response of sap velocity to the environmental variables: Hour, VPD, PAR, Soil VWC, LAI and tree diameter. PAR and VPD were expressed as variations from the respective daytime cycle. Each variable was presented with the relative weight of its variation in that of sap velocity within parentheses. The red dotted lines represent the LOESS smoothing for each response function.

predicted against measured values for the test data set showed that model 1, at low values (up to 30 $cm * h^{-1}$), slightly overestimated half-hourly sap velocity,

otherwise it underestimated sap velocity (Fig. C.1). The *"Fitted functions"* in Figure 6 represents the partial dependencies of sap velocity to the different predictor variables. Furthermore, it was chosen to plot a smoothing of the BRT functions using a LOESS smoothing - the smoothed functions are shown in red (Fig. 6). Once the effect of the daily cycle (Hour), which has a relative influence of 28.0% in explaining sap velocity, was removed, the prevalent environmental variables explaining the variability in sap velocity were PAR above the canopy (21.0%) and VPD (18.5%), followed by soil VWC (16.0%). The evolution of LAI over the season in the two plots explained 8.2% of the variability, while tree diameter, proxy for the different trees, accounted for 8.3% of the total variability.

Sap velocity responded linearly to the variations of VPD around its mean daily cycle (Δ VPD) up to 2 kPa. Beyond this point, the BRT model suggests an increase in the slope of this relationship. The variability in PAR above the canopy was a key driver of sap velocity. When PAR was above-average compared to its mean daily cycle (Δ PAR >0), sap velocity increased with PAR in a linear fashion. For below-average PAR (Δ PAR <0), sap velocity remained relatively stable until Δ PAR reached -500$\mu mol * s^{-1} * m^{-2}$. Beyond this point, the response of sap flow to PAR declined and then stabilized. Sap velocity increased with soil VWC up to 0.24 $m^3 * m^{-3}$ and plateaued until it reached a threshold value of 0.27 $m^3 * m^{-3}$. Beyond this value, sap velocity increased steeply until VWC reached a value of 0.29 $m^3 * m^{-3}$. At a VWC above 0.29 $m^3 * m^{-3}$ the response of sap velocity flattened out until field capacity (0.34 $m^3 * m^{-3}$)(Figure 6). The LAI and tree diameter showed a rather flat relation with sap velocity and were negligible drivers of sap velocity at the sub-daily timescale.

In the sub-daily model, the interactions between VPD and PAR and VPD and LAI were more important than the other interactions (Tab. 1) which means that VPD modified the sap velocity response to both LAI and PAR significantly. When VPD and PAR were low compared to the average daily cycle, sap velocity was very low (Fig. 7). When VPD was high, the sap velocity was very high,

21

	Hour	Diameter	VPD	PAR_Above	LAI	Soil_VWC
Hour	0	15532.81	43578.24	40167	8701.57	13663.24
Diameter	0	0	23831.45	12599.22	10280.22	25915.23
VPD	0	0	0	**82788.32**	**71754.54**	59080.78
PAR_Above	0	0	0	0	35495.65	23574.91
LAI	0	0	0	0	0	27616.26
Soil_VWC	0	0	0	0	0	0

Table 1: Interactions between the variables considered in the BRT Model 1 in explaining cacao sap velocity at a sub daily timescale. For each pair of variables it is reported the mean value of the residuals, whose magnitude represents the strength of any interaction effect. In bold are reported the interactions considered strong, thus significant, by the model.
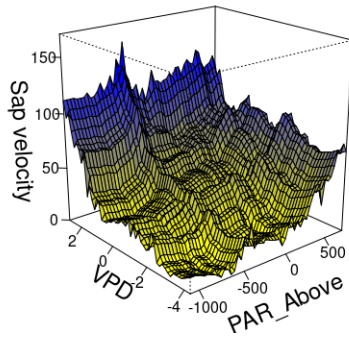

Figure 7: Three-dimensional partial dependence plots for the interaction between VPD (ΔkPa) and PAR ($\Delta \mu mol * s^{-1} * m^{-2}$) variations from the mean daily cycle in the BRT model 1 for half-hourly sap velocity ($cm * h^{-1}$) in cacao trees. All variables except those plotted are held constant at their mean values.
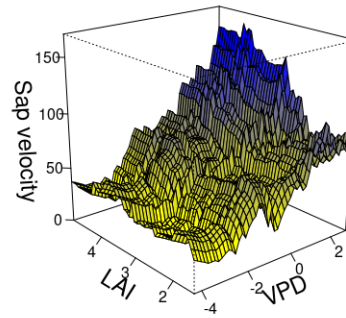
Figure 8: Three-dimensional partial dependence plots for the interaction between LAI ($m^2[leaf] * m^{-2}[soil]$) and VPD (ΔkPa) variation from the mean daily cycle in the BRT model 1 for half-hourly sap velocity ($cm * h^{-1}$) in cacao trees. All variables except those plotted are held constant at their mean values.

for any value of PAR. Similarly, when PAR was high, sap velocity was high and stable whatever the value of VPD, except when VPD was very high, where sap velocity was very high. When VPD and LAI were low, the sap flow was also very low (Fig. 8). When VPD was low, the sap velocity remained low, whatever the value of LAI. When LAI was low (<2.5), sap velocity increased with ~~VPD to a high value. Butwhen~~ the VPD anomaly with the same evolution

22

and reached similar high values for positive VPD anomalies. But, when both LAI and VPD were high ~~, sap velocity increased greatly, indicating that there was a clear~~ (LAI>2.5; VPD anomaly >0), the response of sap velocity was characterized by a steeper slope, indicating a possible positive synergistic effect on sap velocity between VPD and LAI. ~~The~~ This synergy meant that the positive response of sap velocity to positive VPD anomalies (Fig. 6) was amplified by the canopy density when LAI was above 2.5 (Fig. 8). If the LAI alone was not able to sensibly change the sap velocity (Fig. 6), at high values (LAI>2.5) its importance was inflated by positive VPD anomalies (Fig. 8). Ultimately, the sap velocity of trees with an LAI above 2.5 under a stronger pulling force from the atmosphere (positive VPD anomalies) resulted to be higher than the single responses to each of the two predictors alone. Conversely, the potentially interesting interaction between VPD and soil VWC was not found strong enough to be considered relevant according to model 1 (Tab. 1).

3.4. Daily variations of sap velocity in response to climatic drivers

The BRT model based on the daily averages of sap flow velocity rendered a strong training data correlation (0.944), a good cross-validation correlation (0.803). Thus, the model was found to be stable and reliable. An evaluation of predicted against measured values on the test data showed that model 2 predicted well sap velocity despite a slight underestimation at high daily average sap velocities (above 57 $cm * h^{-1}$) (Fig. C.2). Furthermore, when scaling up from the half-hourly to the daily analysis, the weight of the predictors on sap velocity changed (Fig. 9). The variability in daily sap velocity was mostly explained by LAI (27.2%) and soil VWC (21.4%). The relative importance of radiation (PAR) and VPD decreased to 18.1% and 17.0% respectively. 16.3% of the variability in sap velocity was explained by variations in trunk diameter.

The shape of the response curves of daily sap velocity to the considered variables was different to that observed for half-hourly values (Fig. 6, 9). Sap velocity increased nearly linearly with LAI above 3.5 $m^2[leaf] * m^{-2}[soil]$. Sap
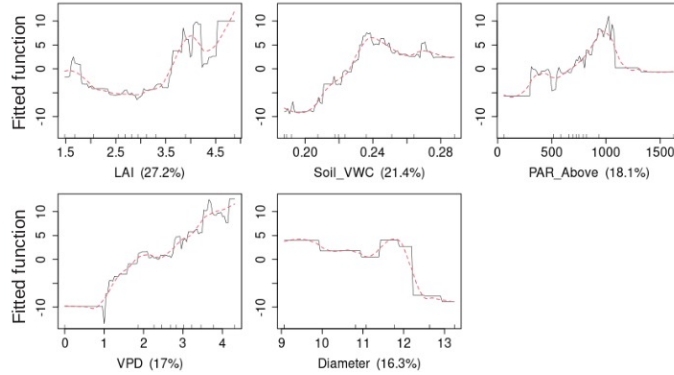
23

Figure 9: Overview of cacao's daily sap velocity response to the main environmental drivers according to a BRT model (model 2). The responses are calculated for daily averages during the entire period of this study. Functional shapes of the response of sap velocity to the environmental variables: VPD, PAR, Soil VWC, LAI and tree diameter. Each variable is presented with the relative importance of its variation on that of sap velocity within parentheses.

505 velocity was insensitive to LAI, for values between 2 and 3.5 $m^2[leaf]*m^{-2}[soil]$.
506 Below $2m^2[leaf] * m^{-2}[soil]$ and down to 1.5 $m^2[leaf] * m^{-2}[soil]$ (minimum
507 value measured in our study), sap flow velocity also responded to changes in
508 LAI, increasing as LAI was lower. Sap flow velocity increased linearly with
509 soil VWC until a threshold level of 0.24 $m^3 * m^{-3}$ (approximately -0.16 MPa
510 for our soil), past which it plateaued. The shape of the response curve of sap
511 velocity to mean daily PAR was almost linear in the range from 0 to 1100
512 $\mu mol * s^{-1} * m^{-2}$. Beyond this value, the response of sap velocity captured by
513 the BRT model leaned on few points, thus was not considered reliable. Finally,
514 the mean daily sap velocity increased linearly with daily average VPD in a sim-
515 ilar fashion to that observed in the half-hourly model 1 (Fig. 6, 9).

516

517 A significant interaction was found between LAI and soil VWC and, to a
518 lesser extent, between VPD and PAR (Tab. 2). When LAI was low, ~~Sap~~ sap
519 velocity increased slightly with soil VWC (Fig. 10). But when LAI reached the
520 value of 3 $m^2 * m^{-2}$, the increase with soil VWC became much more important
521 and sap velocity ~~reaches~~ reached very high values. The interaction between

24

	PAR_Above	LAI	Soil_VWC	VPD	Diameter
PAR_Above	0	2692.77	340.99	**5507.51**	4970.65
LAI	0	0	**19350.06**	5019.99	5275.63
Soil_VWC	0	0	0	510.93	1408.86
VPD	0	0	0	0	2304.21
Diameter	0	0	0	0	0

Table 2: Interactions between the variables considered in the BRT Model 2 in explaining cacao sap velocity at the scale of one day. For each pair of variables it is reported the mean value of the residuals, whose magnitude represents the strength of any interaction effect. In bold are reported the interactions considered strong, thus significant, by the model.

average daily VPD and PAR, although less pronounced, showed that the increase in VPD and PAR may have a synergistic effect on sap velocity (Fig. 11). As PAR increased (up to 1100 $mumol * s^{-1} * m^{-2}$) sap velocity responded more readily to daily average VPD and vice versa. Few PAR values were recorded above 1100 $mumol * s^{-1} * m^{-2}$ and the apparent decrease in sap velocity after this value was not interpretable. At the one-day time scale, no interaction between mean soil VWC and VPD was detected by model 2 (Tab. 2), similarly to what was found at the sub-day level (Tab. 1).

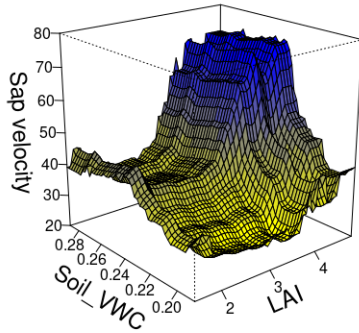Figure 10: Three-dimensional partial dependence plots for the interaction between soil VWC ($m^3 * m^{-3}$) and LAI ($m^2[leaf] * m^{-2}[soil]$) in the BRT model 2 for daily average sap velocity ($cm * h^{-1}$) in cacao trees. All variables except those plotted are held constant at their mean values.

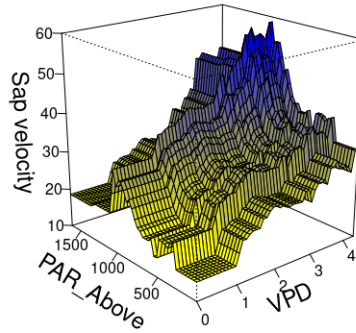Figure 11: Three-dimensional partial dependence plots for the interaction between PAR ($\mu mol * s^{-1} * m^{-2}$) and VPD ($kPa$) in the BRT model 2 for daily average sap velocity ($cm * h^{-1}$) in cacao trees. All variables except those plotted are held constant at their mean values.

25

4. Discussion

4.1. Climate

The measured climate of the 2019-2020 dry season (Fig. 2) was representative for the conditions experienced by cacao during this time of the year in the Eastern region of Ghana. As soil VWC approached the wilting point in the control plot, air humidity dropped even below 20% and temperatures were sub-optimal (Fig. 2, Fig. A.1), on a daily basis, the measured conditions were found to be stressful according to the definitions given for soil and atmospheric stresses (see Section 1).

4.2. Canopy

Despite the occurrence of high temperatures, the trees were able to cope with the climate in December. We argue so because we did not observe any decline in LAI in either watering treatment, in line with previous studies with no atmospheric stress [67, 19]. Leaf shedding is a common response to drought of tropical and subtropical species [68, 69], as it allows trees to reduce transpiration rates and, hence, avoid hydraulic failure. In line with the idea that cacao trees apply this drought-coping strategy, during the more severe part of the dry season (from January onwards), LAI decreased in both watering treatments, although at a faster rate in the control plot (Fig. 3), supporting the idea that leaf shedding helps cacao to cope with soil drought. However, given that LAI also decreased in the irrigated plot throughout the experimental period, it is likely that trees in the irrigated plot also suffered from water stress. It could be argued that the irrigation level (60 L/tree on alternate days equivalent to approximately 9.6 mm of rain) was not sufficient to completely mitigate soil drought (Fig. 2), despite being in line with the water requirement of a mature tree found in literature [37].

Alternatively, it can be interpreted as the atmospheric drought having con-tributed to leaf shedding. This latter interpretation is supported by the more abundant litter production observed in December, when the soil VWC was sig-nificantly higher in the irrigated plot than in the control but air humidity and

temperature reached values above stressful thresholds (Fig. A.1, B.2). The timing of the drop in LAI suggests that the key atmospheric condition impacting the canopy was the extremely low air humidity to which cacao leaves might not be adapted, especially considering that cacao developed under very high relative air humidity [70].

By the end of the dry season, the control plot had lost two thirds of its foliage, twice the loss in the irrigated plot. In light of the lack of interaction between VPD and soil VWC in explaining sap velocity (Tab. 1, 2) it could be assumed that the effects of atmospheric and soil stress on LAI were independent. If this assumption is accepted, the difference in LAI drop between the two plots must have been driven by the difference in soil VWC (Fig. 2, 3). The fact that the net loss in LAI in the control relative to that in the irrigated treatment (-62.5% vs. -32.5% over the course of the experiment, respectively) was much larger than the difference in litterfall between the two treatments (309 $g[dry] * m^{-2}$ and 247 $g[dry] * m^{-2}$, respectively - a relative difference of 25%) suggests that some leaf flushing might have occurred in the irrigated treatment. This hypothetical leaf flushing in the irrigated treatment never sufficed to counterbalance the leaf shedding, possibly due to a limitation in carbon to invest in leaf production, resulting in a drop in LAI. Further, more specific, studies to investigate the effects of atmospheric and soil drought on leaf flushing dynamics would be needed in order to properly characterize such effects.

~~Based~~ It is acknowledged that the irrigation might have been sub-optimal but, based on the above reasoning, the loss of canopy density in the irrigated plot was imputable ~~only~~ mostly to the atmospheric stress~~, while in~~. In the control the additional loss was caused by the soil stress and the interaction between the two stresses, if present. Thus, our results on the LAI evolution and litterfall production show that the impact of atmospheric stress (VPD) on the canopy during the dry Harmattan season may be of similar magnitude, if not greater, than that of soil stress (soil VWC), regardless of the possible interaction between the two stresses (Fig. 3). If the two stresses were independent then the depressing effects of soil and atmospheric stress were the same, one third of the initial

canopy density each. While the existence of an interaction between the two would mean that the soil stress impacted the canopy less than the atmospheric one. The major role found for the aerial stress is in line with Hutcheon at al. (1973) [71], who concluded that the beneficial effect of irrigation on cacao total biomass production was limited when in presence of atmospheric stress. Other authors reported the same [17, 37] but, to our knowledge, this was the first attempt to quantify the effects under field conditions in West Africa. Our results contrast with those from a study in which LAI did not change in response to a 73% reduction in precipitation over 13 months [19]. It must be noted that the experimental conditions between this experimental site in Sulawesi, Indonesia and ours in Eastern Ghana differ greatly. For the site in Sulawesi, it was suggested that the reduction in incoming precipitation was insufficient to impose stressful conditions due to the high mean annual rainfall (2,844 mm) [72]. Furthermore, at the Indonesian site, daily mean relative air humidity never dropped below 69%, in contrast to our study site, where relative air humidity often fell below 40%, and where we found a significant drop in LAI, irrespective of the irrigation regime.

4.3. Sap velocity

The two models developed (half-hourly: BRT model 1, daily: BRT model 2) allowed us to obtain a good estimate of the environmental and climatic drivers of sap velocity on a half-hourly and daily scale. This allowed an effective investigation of the impacts of atmospheric and soil water stress on cacao during Harmattan season. Up to now, in cacao, the response of transpiration to atmospheric drought stress had only been studied under controlled conditions, in young individuals and never in combination with limited water availability [13, 14, 15]. Previous studies addressing the effects of climatic factors (VPD, soil VWC and PAR mainly) on transpiration did not find clear patterns [13, 17]. Fraga et al. 2020 [13] argued that large temporal and spatial heterogeneity, mainly in VPD and soil water, could account for some of the unexplained variability in transpiration. We argue that our approach of separating the instantaneous half-hourly

effect from the integrated daily effects allowed us to disentangle some of these patterns. Furthermore, to our knowledge, this is the first study that addressed the effect of the interactions among variables on sap velocity.

Soil VWC and LAI did not change significantly at the time scale of one day. Despite their lack of variation at the sub-daily level, soil VWC and LAI varied over the season, setting different daily conditions for sap velocity variation in response to the variability of the remaining variables (PAR, VPD) (Fig. 4,5,6). The BRT model 1 showed that of these two conditions, soil VWC mattered more than LAI (Fig. 6). This suggests that water availability matters more than the total leaf area available for transpiration in determining sap velocity. In cacao the transpiration is largely performed in the outer crown, while the shade leaves are far less active [17, 67]. The loss of foliage probably interested mostly sun leaves [67] but the trees were probably able to adapt the lower strata of the canopy to the new conditions [73, 74], minimizing the direct effect of LAI on sub-daily sap velocity. This was reflected in the flat response of sap velocity to LAI in model 1 (Fig. 6). Instead, the different soil VWC over the season appeared to matter more in determining the sub-daily sap velocity possibly hinting that cacao might be more limited by its root water uptake and by the conductivity of the vascular system rather than by the canopy conductance, in line with [16].

Within a day, sap velocity responded mainly to the variation of PAR and VPD and their synergistic effects (Fig. 7). At the sub-daily time scale, PAR was the principal driver for sap velocity, as long as VPD did not exceed the mean daily cycle by more than 2 kPa. Beyond this value for the anomaly, it is possible that for most part of the day stomatal regulation was no longer effective in dealing with the high water demand from the atmosphere. This is supported by the fact that irrigation was not able to limit water loss when VPD was extremely high and the trees ended up transpiring as much as the control plot (Fig. 5 A). Moreover, the observed peak in sap velocity up to 20 cm/h in the morning cannot be explained by the extremely low values of VPD and PAR (Fig. 5 A, B). However, said peak may be explained as a phenomenon of recovery from

29

embolism [75]. It has been described in other plants that, following embolism due to hydraulic stress, the plant applies a positive root pressure to force the gas to dissolve. Such recovery strategy of embolism removal is often put in place concurrently to the start of transpiration in the morning [76, 77, 75]. The control trees, constantly stressed by the low VWC, may have had to adopt this strategy regardless of the VPD level, as the early morning peak in sap velocity suggests (Fig. 5 A,B). The irrigated trees did not present the same peak in the early morning in days with moderate-low average VPD but irrigation might have not prevented embolism when VPD was high, leading to an early morning sap velocity peak compatible with the refilling of vases (Fig. 5 A, B). This behaviour is an ulterior element in favour of the fact that irrigation is not sufficient when the atmospheric stress is too strong. Cacao plants naturally occur in the understorey of tropical forests, where light is limited and VPD is rarely high [78]. Hence, we could expect that stomatal behavior is finely-tuned in cacao to respond to variations in light availability, to maximize photosynthesis [74, 79], but it might not be adapted to regulate water loss under increasing VPD, as we observed in our experiment (Fig. 4). Before this study, the atmospheric component of water stress had rarely been taken into account because such conditions are seldom met in most of the cacao-growing areas worldwide [18, 72]. Nonetheless, most of the West African cacao belt undergoes atmospheric stress on a quasi-seasonal basis under the influence of the Harmattan winds [23] and the chances of harsher atmospheric stress in the region will increase with climate change cite. Given that west Africa includes the two leader of cacao production worldwide (Ivory Coast and Ghana) [80], it should be recognized the due importance to the atmospheric stress.

At the seasonal time scale (effects on daily averages), the effects of PAR and VPD, as well as their interaction, were maintained but, at this time scale ,. It is possible that under high VPD, the plants were inclined to transpire more anyway (Fig. 9) but, with increasing levels of PAR, it may have had more reason to do so. It is presumable that, especially in the deeper canopy layers, the need to collect more CO_2 rose. Similarly, with increasing radiation and photosynthesis

30

it is possible that the plant kept its stomata open to cool the leaves down, becoming more responsive to VPD.

Together with PAR and VPD, at the seasonal time scale soil VWC played a major role as well (Fig. 9, 11). The response curve of sap velocity to soil VWC in figure 9 highlights that, under our experimental conditions, the soil reached a critical soil VWC at which cacao water extraction capacity was challenged (0.24 $m^3 * m^{-3}$, approximately -0.16 MPa for our soil). A significantly lower critical value of soil water potential for water extraction (-0.079 MPa) has previously been reported for young cacao plants under field conditions in Brazil [13]. The difference between the Brazilian study and ours is possibly related to the differences in genetics, age, and rooting depth considered in the two experiments. Here, we studied mature trees subject to water stress on a regular basis every year. These two elements (age and prevailing climate) imply that our trees would have had a more developed rooting system, capable of exploring a larger soil volume.

Contrary to our initial expectations, our results from the BRT models did not clearly show an interactive effect between atmospheric and soil drought on cacao transpiration, represented in the models by VPD and soil VWC (Tab. 1, 2). Yet, our results cannot completely rule out our initial hypothesis as, for example, Model 1 highlighted a not significant but strong link between VPD and soil VWC (Tab. 1). The BRT models could have failed at capturing such interaction because of the paucity of observations when atmospheric and soil drought co-occurred in the control plot, a key requirement to train the model. Furthermore, the provided level of irrigation might have not been sufficient to completely alleviate the soil stress in the irrigated part. If this was the case, the small Δ VWC between plots might have made more complicated for the model to capture an interaction between soil and atmospheric drought across treatments as well.

At the seasonal time-scale (daily average measurements), we found that the response of sap velocity to both atmospheric and soil drought was modulated by the interaction with LAI. We found that beyond certain threshold values of both

31

VWC ($0.24\ m^3 * m^{-3}$) and LAI ($3.5\ m^2[leaf] * m^{-2}[soil]$), sap velocity did not respond to further increases in either variable. The daily average sap velocity measured under these conditions, high VWC and LAI($76\ cm * h^{-1}$), could be the maximum supported by the root and vascular system of cacao, although this should be further tested in other climates. When soil VWC was below 0.24 $m^3 * m^{-3}$, sap velocity was strongly responsive to soil VWC variations, regardless of the LAI, whereas for a given soil VWC, the response of sap velocity to changes in LAI was less pronounced (Fig. 10). This behaviour is compatible with the higher importance of soil VWC over LAI found in model 1 (Fig. 6) and with the more dynamic shape for the response of sap velocity to soil VWC and flatter one for LAI in model 1 (Fig. 6) and for most of the range (1.5 to 3.5) in model 2 (Fig. 9). Furthermore, the irrigated trees only showed signs of probable embolism recovery in the mornings of days with a high VPD, suggesting that they were not able to uptake enough water from the soil to avoid embolism (Fig. 5 A). While in the control the morning peak in sap velocity, that we proposed as a sign of embolism recovery, was present with approximately the same magnitude under high and low VPD (Fig. 5 A,B). This suggests that the main limitation for water transportation in the soil-plant-atmosphere continuum was found in the ability of the plant to extract water from the soil. The results discussed in this paragraph sustain the theory that cacao's transpiration is mostly limited by the root water uptake capacity rather than by the conductivity of the vascular system or the total leaf area, in line with [16].

5. Conclusions

For the first time, in this study, we assessed the effects of soil and atmospheric water stress on canopy transpiration of adult cocoa trees. We showed that under high soil and atmospheric water stress, irrigation decreased leaf shedding in response to limited water availability in the soil. Nonetheless, under a climate change scenario with harsher conditions experienced by cacao under the influence of the Harmattan winds, irrigation might not suffice to sustain cacao

32

production. In fact, our study highlights that cacao transpiration increases with high VPD, which could further compromise soil water availability and eventually aggravate soil stress. The use of shade nets or of shade trees with a deep rooting system, as previously suggested [81, 82], could be a key requirement for cacao farming in the future to partially alleviate atmospheric drought stress. Deep-rooted vegetation and/or shading nets diminish the detrimental impact of increased atmospheric drought by buffering temperature and relative air humidity. This prevents stressful values for temperature and relative air humidity without adding competition for water extraction. Still, to predict the actual impact of increased drought severity under climate change on cacao production, it will be necessary to look beyond the effects of soil and atmospheric drought on transpiration and leaf area, and study how these conditions affect flower, fruit and seed production in the field. Furthermore, other similar studies are needed to validate and strengthen these conclusions, which rely on data with limited replicates that may limit the possibility of generalizing these findings for other situations. In any case, this study has confirmed in the field what previous studies had found in controlled environment and proposed new results that are in line with the behaviour in similar environments of cacao and other species.
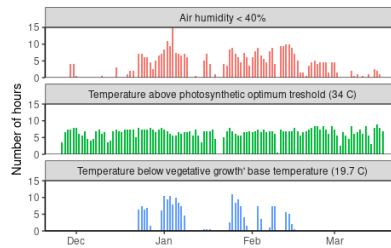
Appendix A. Atmospheric stressors

Figure A.1: Number of hours per day under stressful climatic conditions for cacao trees according to values reported in [17, 26, 27, 28, 21]; each bar is one day. Top: air humidity below 40%; middle: temperature above photosynthetic optimum threshold (34 °C); bottom: temperature below the base temperature for vegetative growth (19.7 °C).
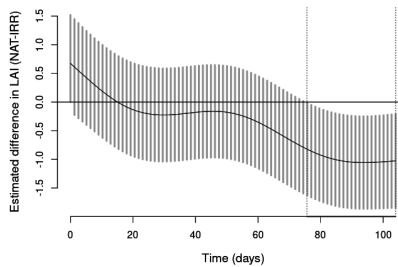
Appendix B. Leaf area index

Figure B.1: Difference in estimated leaf area index (LAI) between the irrigated and the control plot. The fitted line is a generalized additive model and the shaded area is the 95% prediction interval. A shaded area non-overlapping with the zero-line indicates a significant difference between watering treatments.
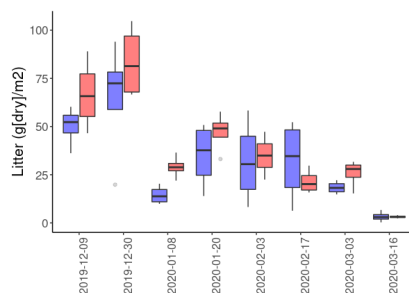
Figure B.2: Litter production of cacao trees during the dry Harmattan season, in presence (blue) and absence (red) of irrigation. Box-plots represent variations between the four litter traps per treatment and date. Bold lines represent means per plot and date.

Appendix C. Boosted Regression Trees analysis

Appendix C.1. parameterization of the models

	Step	Family	tl	bg	nt	tc	lr
Model 1	30 min	Gauss	0.01	0.75	100	3	0.1
Model 2	1 day	Gauss	0.001	0.75	100	3	0.05

Table C.3: Parametrization of the BRT models to predict the transpiration during the day at a 30-minute time interval (Model 1) and at a daily time step (Model 2). A BRT model requires the definition of a set of hyperparameters:

family - the type of statistical error distribution characterizing the data, in our case Gaussian;

tolerance (tl) - the threshold in variance change under which to stop the model reiteration;

bag fraction (bg) - the fraction of dataset to use for the training of each tree. The remaining data is used at each step to cross validate the set of relations found;

number of trees (nt) - the number of trees necessary for optimal prediction. It is determined based on tl and bg;

tree complexity (tc) - the maximum level of interaction between variables to consider in a tree;

learning rate (lr) - determines the contribution of each tree to the growing model.

The seed number used was - 210920.

Appendix C.2. Evaluation of BRT models on the test data

To allow an independent evaluation of the BRT models, 25% of the field data was set aside to be used as a test subset of data and was not used at any

36

point in the training of the BRT models. This section of the appendix presents the evaluation of the models (Model 1, Model 2) on this test data subset.
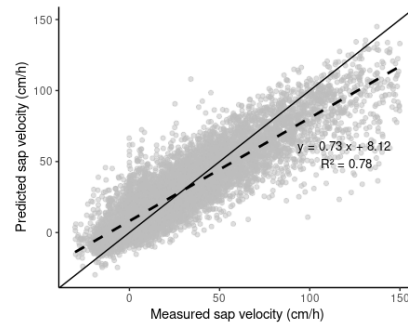

Figure C.1: Observed (abscissa) vs. predicted (ordinates) sap velocity, the corresponding linear regression (dashed line) and y=x line (full black line) for the BRT half-hourly model (model 1) test data.
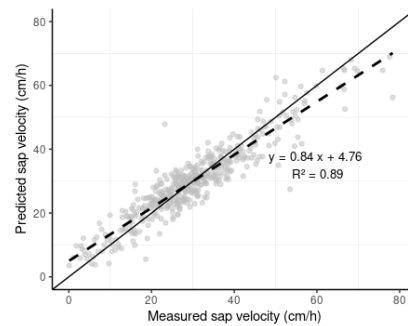

Figure C.2: Observed (abscissa) vs. predicted (ordinates) sap velocity, the corresponding linear regression (dashed line) and y=x line (full black line) for the BRT daily model (model 2) test data.

References

[1] I. P. O. C. C. (IPCC), The IPCC'S Fifth Assessment Report; What's in it for Africa, Change (2014).

[2] J. A. van Vliet, K. E. Giller, Mineral Nutrition of Co-coa: A Review, volume 141, 1 ed., Elsevier Inc., 2017. URL: http://dx.doi.org/10.1016/bs.agron.2016.10.017. doi:10.1016/bs.agron.2016.10.017.

[3] M. K. Van Ittersum, L. G. Van Bussel, J. Wolf, P. Grassini, J. Van Wart, N. Guilpart, L. Claessens, H. De Groot, K. Wiebe, D. Mason-D'Croz, H. Yang, H. Boogaard, P. A. Van Oort, M. P. Van Loon, K. Saito, O. Adimo, S. Adjei-Nsiah, A. Agali, A. Bala, R. Chikowo, K. Kaizzi, M. Kouressy, J. H. Makoi, K. Ouattara, K. Tesfaye, K. G. Cassman, Can sub-Saharan Africa feed itself?, Proceedings of the National Academy of Sciences of the United States of America (2016). doi:10.1073/pnas.1610359113.

[4] B. Sultan, M. Gaetani, Agriculture in West Africa in the twenty-first century: Climate change and impacts scenarios, and potential for adaptation, 2016. doi:10.3389/fpls.2016.01262.

[5] G. Schroth, P. Läderach, A. I. Martinez-Valle, C. Bunn, L. Jassogne, Vulnerability to climate change of cocoa in West Africa: Patterns, opportunities and limits to adaptation, Science of the Total Environment 556 (2016) 231–241. doi:10.1016/j.scitotenv.2016.03.024.

[6] P. Läderach, A. Martinez-Valle, G. Schroth, N. Castro, Predicting the future climatic suitability for cocoa farming of the world's leading producer countries, Ghana and Côte d'Ivoire, Climatic Change 119 (2013) 841–854. doi:10.1007/s10584-013-0774-8.

[7] Y. Malhi, J. Wright, Spatial patterns and recent trends in the climate

38

of tropical rainforest regions, in: Philosophical Transactions of the Royal Society B: Biological Sciences, 2004. doi:10.1098/rstb.2003.1433.

[8] N. Nakicenovic, J. Alcamo, A. Grubler, K. Riahi, R. Roehrl, H.-H. Rogner, N. Victor, Special report on emissions scenarios (SRES), a special report of Working Group III of the intergovernmental panel on climate change, Cambridge University Press, 2000.

[9] I. Abdulai, M. P. Hoffmann, L. Jassogne, R. Asare, S. Graefe, H. H. Tao, S. Muilerman, P. Vaast, P. Van Asten, P. Läderach, R. P. Rötter, Variations in yield gaps of smallholder cocoa systems and the main determining factors along a climate gradient in Ghana, Agricultural Systems 181 (2020). doi:10.1016/j.agsy.2020.102812.

[10] K. Schepanski, B. Heinold, I. Tegen, Harmattan, saharan heat low, and west african monsoon circulation: Modulations on the saharan dust outflow towards the north atlantic, Atmospheric Chemistry and Physics 17 (2017) 10223–10243. doi:10.5194/acp-17-10223-2017.

[11] J.-P. Lafore, C. Flamant, F. Guichard, D. J. Parker, D. Bouniol, a. H. Fink, V. Giraud, M. Gosset, N. Hall, H. Höller, S. C. Jones, A. Protat, R. Roca, F. Roux, F. Saïd, C. Thorncroft, Progress in understanding of weather systems in West Africa, Atmospheric Science Letters 12 (2011) 7–12. URL: http://doi.wiley.com/10.1002/asl.335. doi:10.1002/asl.335.

[12] G. Wood, R. Lass, Cocoa, 2001. doi:10.1002/9780470698983.

[13] L. S. Fraga Junior, L. M. Vellame, A. S. de Oliveira, V. P. da Silva Paz, A. S. de Oliveira, V. P. d. S. Paz, Transpiration of young cocoa trees under soil water restriction, Scientia Agricola 78 (2020). doi:10.1590/1678-992x-2019-0093.

[14] J. De Almeida, W. Tezara, A. Herrera, Physiological responses to drought and experimental water deficit and waterlogging of four clones of cacao

835   (Theobroma cacao L.) selected for cultivation in Venezuela, Agricultural
836   Water Management 171 (2016) 80–88. doi:10.1016/j.agwat.2016.03.012.

837 [15] R. L. Melnick, Cherelle wilt of cacao: A physiological condition, in: Cacao
838   Diseases: A History of Old Enemies and New Encounters, 2016, pp. 483–
839   499. doi:10.1007/978-3-319-24789-2_15. arXiv:1011.1669.

840 [16] M. M. Kotowska, D. Hertel, Y. A. Rajab, H. Barus, B. Schuldt, Patterns
841   in hydraulic architecture from roots to branches in six tropical tree species
842   from cacao agroforestry and their relation to wood density and stem growth,
843   Frontiers in Plant Science 6 (2015) 1–16. doi:10.3389/fpls.2015.00191.

844 [17] F. Lahive, P. Hadley, A. J. Daymond, The physiological responses of
845   cacao to the environment and the implications for climate change re-
846   silience . a review, Agronomy for Sustainable Development 39 (2019) 1–22.
847   doi:10.1007/s13593-018-0552-0.

848 [18] L. Schwendenmann, E. Veldkamp, G. Moser, D. Hölscher, M. Köhler,
849   Y. Clough, I. Anas, G. Djajakirana, S. Erasmi, D. Hertel, D. Leitner,
850   C. Leuschner, B. Michalzik, P. Propastin, A. Tjoa, T. Tscharntke, O. van
851   Straaten, Effects of an experimental drought on the functioning of a cacao
852   agroforestry system, sulawesi, indonesia, Global Change Biology (2010).
853   doi:10.1111/j.1365-2486.2009.02034.x.

854 [19] G. Moser, C. Leuschner, D. Hertel, D. Hölscher, M. Köhler, D. Leitner,
855   B. Michalzik, E. Prihastanti, S. Tjitrosemito, L. Schwendenmann, Re-
856   sponse of cocoa trees (theobroma cacao) to a 13-month desiccation pe-
857   riod in sulawesi, indonesia, Agroforestry Systems 79 (2010) 171–187.
858   doi:10.1007/s10457-010-9303-1.

859 [20] T. Najihah, M. Ibrahim, P. Hadley, A. Daymond, The Effect of Different
860   Day and Night Temperatures on the Growth and Physiology of Theobroma
861   cacao under Controlled Environment Condition, Annual Research & Re-
862   view in Biology 27 (2018) 1–15. doi:10.9734/arrb/2018/40413.

[21] A. J. Daymond, P. Hadley, The effects of temperature and light integral on early vegetative growth and chlorophyll fluorescence of four contrasting genotypes of cacao (Theobroma cacao), Annals of Applied Biology 145 (2004) 257–262. doi:doi:10.1111/j.1744-7348.2004.tb00381.x.

[22] R. A. Asare, R. Asare, W. A. Asante, B. Markussen, A. RÆbild, IN-FLUENCES of SHADING and FERTILIZATION on ON-FARM YIELDS of COCOA in GHANA, Experimental Agriculture 53 (2017) 416–431. doi:10.1017/S0014479716000466.

[23] I. Abdulai, P. Vaast, M. P. Hoffmann, R. Asare, L. Jassogne, P. Van Asten, R. P. Rötter, S. Graefe, Cocoa agroforestry is less resilient to sub-optimal and extreme climate than cocoa in full sun, Global Change Biology 24 (2018) 273–286. doi:10.1111/gcb.13885.

[24] J. Jenik, J. B. Hall, The Ecological Effects of the Harmattan Wind in the Djebobo Massif (Togo Mountains, Ghana), The Journal of Ecology (1966). doi:10.2307/2257816.

[25] J. K. Hagan, M. Bosompem, I. A. Adjei, The productive performance of local chickens in three ecological zones of Ghana., Journal of Agricultural and Biological Science 8 (2013) 51–56.

[26] P. G. Oguntunde, Whole-plant water use and canopy conductance of cassava under iimited available soil water and varying evaporative demand, Plant and Soil 278 (2005) 371–383. doi:10.1007/s11104-005-0375-z.

[27] F. C. Meinzer, Functional convergence in plant responses to the environment, Oecologia 134 (2003) 1–11. doi:10.1007/s00442-002-1088-0.

[28] A. R. GOMES, T. T. KOZLOWSKI, P. B. REICH, Some Physiological Responses of Theobroma Cacao Var. Catongo Seedlings To Air Humidity, New Phytologist 107 (1987) 591–602. doi:10.1111/j.1469-8137.1987.tb02929.x.

[29] S. P. Long, C. J. Bernacchi, Gas exchange measurements, what can they tell us about the underlying limitations to photosynthesis? Procedures and

891   sources of error, Journal of Experimental Botany 54 (2003) 2393–2401.
892   doi:10.1093/jxb/erg262.

893 [30] M. M. Chaves, J. P. Maroco, J. S. Pereira, Understanding plant responses
894   to drought - From genes to the whole plant, Functional Plant Biology 30
895   (2003) 239–264. doi:10.1071/FP02076.

896 [31] B. E. Medlyn, R. A. Duursma, D. Eamus, D. S. Ellsworth, I. C. Prentice,
897   C. V. Barton, K. Y. Crous, P. De Angelis, M. Freeman, L. Wingate, Rec-
898   onciling the optimal and empirical approaches to modelling stomatal con-
899   ductance, Global Change Biology 17 (2011) 2134–2144. doi:10.1111/j.1365-
900   2486.2010.02375.x.

901 [32] J. Yang, R. A. Duursma, M. G. De Kauwe, D. Kumarathunge, M. Jiang,
902   K. Mahmud, T. E. Gimeno, K. Y. Crous, D. S. Ellsworth, J. Peters, et al.,
903   Incorporating non-stomatal limitation improves the performance of leaf and
904   canopy models at high vapour pressure deficit, Tree physiology 39 (2019)
905   1961–1974.

906 [33] N. Martin-StPaul, S. Delzon, H. Cochard, Plant resistance to drought
907   depends on timely stomatal closure, Ecology Letters 20 (2017) 1437–1447.
908   doi:10.1111/ele.12851.

909 [34] U. Hochberg, F. E. Rockwell, N. M. Holbrook, H. Cochard,
910   Iso/Anisohydry: A Plant–Environment Interaction Rather Than a
911   Simple Hydraulic Trait, Trends in Plant Science 23 (2018)
912   112–120. URL: http://dx.doi.org/10.1016/j.tplants.2017.11.002.
913   doi:10.1016/j.tplants.2017.11.002.

914 [35] R. Machado, L. Loram-Lourenço, F. S. Farnese, R. D. F. B. Alves, L. F.
915   de Sousa, F. G. Silva, S. C. V. Filho, J. M. Torres-Ruiz, H. Cochard,
916   P. E. Menezes-Silva, Where do leaf water leaks come from? Trade-offs
917   underlying the variability in minimum conductance across tropical savanna
918   species with contrasting growth strategies, New Phytologist (2020) 0–3.
919   doi:10.1111/nph.16941.

[36] G. Egea, A. Verhoef, P. L. Vidale, Towards an improved and more flexible representation of water stress in coupled photosynthesis-stomatal conductance models, Agricultural and Forest Meteorology 151 (2011) 1370–1384. doi:10.1016/j.agrformet.2011.05.019.

[37] M. K. V. Carr, G. Lockwood, The water relations and irrigation requirements of cocoa (Theobroma cacao L.): A review, Experimental Agriculture 47 (2011) 653–676. doi:10.1017/S0014479711000421.

[38] A. J. Daymond, P. Hadley, Differential effects of temperature on fruit development and bean quality of contrasting genotypes of cacao (Theobroma cacao), Annals of Applied Biology 153 (2008) 175–185. doi:10.1111/j.1744-7348.2008.00246.x.

[39] G. J. Anim-Kwapong, E. B. Frimpong, Vulnerability and Adaptation Assessment Under the Netherlands Climate Change Studies Assistance Programme Phase 2 (NCCSAP2), Cocoa Research Institute of Ghana 2 (2008) 1–30.

[40] N. C. for Atmospheric Research Staff, Climate data sets: Ncar - climate data guide, 2015. URL: https://climatedataguide.ucar.edu/climate-data/cpc-unified-gauge-based-analysis-global-d

[41] D. C. Marshall, Measurement of Sap Flow in Conifers by Heat Transport., Plant Physiology (1958). doi:10.1104/pp.33.6.385.

[42] M. Forster, The Dual Method Approach (DMA) Resolves Measurement Range Limitations of Heat Pulse Velocity Sap Flow Sensors, Forests 10 (2019) 46. URL: http://www.mdpi.com/1999-4907/10/1/46. doi:10.3390/f10010046.

[43] Y. COHEN, M. FUCHS, G. C. GREEN, Improvement of the heat pulse method for determining sap flow in trees, Plant, Cell & Environment (1981). doi:10.1111/j.1365-3040.1981.tb02117.x.

[44] S. S. Burgess, M. A. Adams, N. C. Turner, C. R. Beverly, C. K. Ong, A. A. Khan, T. M. Bleby, An improved heat pulse method to measure low and reverse rates of sap flow in woody plants, Tree Physiology (2001). doi:10.1093/treephys/21.9.589.

[45] T. M. Bleby, S. S. Burgess, M. A. Adams, A validation, comparison and error analysis of two heat-pulse methods for measuring sap flow in Eucalyptus marginata saplings, Functional Plant Biology (2004). doi:10.1071/FP04013.

[46] M. T. Van Genuchten, A closed-form equation for predicting the hydraulic conductivity of unsaturated soils, Soil science society of America journal 44 (1980) 892–898.

[47] A. R. da Silva, R. P. de Lima, Soilphysics: An R package to determine soil preconsolidation pressure, Computers and Geosciences (2015). doi:10.1016/j.cageo.2015.08.008.

[48] G. S. Campbell, Extinction coefficients for radiation in plant canopies calculated using an ellipsoidal inclination angle distribution 36 (1986) 317–321.

[49] G. N. Flerchinger, Q. Yu, Simplified expressions for radiation scattering in canopies with ellipsoidal leaf angle distributions, Agricultural and Forest Meteorology 144 (2007) 230–235. doi:10.1016/j.agrformet.2007.03.002.

[50] S. C. Thomas, W. E. Winner, A rotated ellipsoidal angle density function improves estimation of foliage inclination distributions in forest canopies, Agricultural and Forest Meteorology 100 (2000) 19–24. doi:10.1016/S0168-1923(99)00089-1.

[51] D. S. Stoffer, P. Bloomfield, Fourier analysis of time series: An introduction, Journal of the American Statistical Association (2000). doi:10.2307/2669794.

[52] P. J. Brockwell, R. A. Davis, S. E. Fienberg, Time series: theory and methods: theory and methods, Springer Science & Business Media, 1991.

[53] W. Rasband, ImageJ, U.S. National Institutes of Health, Bethesda, Maryland, USA, 2014.

[54] R. G. Allen, L. S. Pereira, D. Raes, M. Smith, W. Ab, Fao,1998, Irrigation and Drainage Paper No. 56, FAO (1998) 300. doi:10.1016/j.eja.2010.12.001.

[55] J. A. J. Berni, P. Zarco-Tejada, G. Sepulcre-Canto, E. Fereres, F. Villalobos, Mapping canopy conductance and cwsi in olive orchards using high resolution thermal remote sensing imagery, Remote Sensing of Environment 113 (2009) 2380–2388. doi:10.1016/j.rse.2009.06.018.

[56] R Core Team, R: A Language and Environment for Statistical Computing, R Foundation for Statistical Computing, Vienna, Austria, 2019. URL: https://www.R-project.org/.

[57] H. Wickham, The split-apply-combine strategy for data analysis, Journal of Statistical Software 40 (2011) 1–29.

[58] H. Wickham, M. Averick, J. Bryan, W. Chang, L. D. McGowan, R. François, G. Grolemund, A. Hayes, L. Henry, J. Hester, M. Kuhn, T. L. Pedersen, E. Miller, S. M. Bache, K. Müller, J. Ooms, D. Robinson, D. P. Seidel, V. Spinu, K. Takahashi, D. Vaughan, C. Wilke, K. Woo, H. Yutani, Welcome to the tidyverse, Journal of Open Source Software 4 (2019) 1686. doi:10.21105/joss.01686.

[59] S. Wood, Generalized Additive Models: An Introduction with R, 2 ed., Chapman and Hall/CRC, 2017.

[60] J. van Rij, M. Wieling, R. H. Baayen, H. van Rijn, itsadug: Interpreting time series and autocorrelated data using gamms, 2017. R package version 2.3.

[61] J. Elith, J. R. Leathwick, T. Hastie, A working guide to boosted regression trees, 2008. doi:10.1111/j.1365-2656.2008.01390.x.

[62] G. De'ath, K. E. Fabricius, Classification and regression trees: a powerful yet simple technique for ecological data analysis, Ecology 81 (2000) 3178–3192.

[63] R. E. Schapire, The boosting approach to machine learning: An overview, in: Nonlinear estimation and classification, Springer, 2003, pp. 149–171.

[64] J. Elith, J. Leathwick, Boosted Regression Trees for ecological modeling (2011) 1–22.

[65] B. Greenwell, B. Boehmke, J. Cunningham, D. GBM, gbm: generalized boosted regression models. r package version 2.1. 5, Available at R Core Team https://CRAN. R-project. org/package= gbm [Verified 16 June 2018] (2018).

[66] R. J. Hijmans, S. Phillips, J. Leathwick, J. Elith, M. R. J. Hijmans, Package 'dismo' (2017).

[67] A. K.-i. Miyaji, W. S. Silva, P. D. T. Alvim, Productivity of Leaves of a Tropical Tree, Theobroma cacao, Grown Under Shading, in Relation to Leaf Age and Light Conditions within the Canopy 137 (1997) 463–472.

[68] S. J. Bucci, F. G. Scholz, P. I. Campanello, L. Montti, M. Jimenez-Castillo, F. A. Rockwell, L. L. Manna, P. Guerra, P. L. Bernal, O. Troncoso, J. Enricci, M. N. Holbrook, G. Goldstein, Hydraulic differences along the water transport system of South American Nothofagus species: Do leaves protect the stem functionality?, Tree Physiology 32 (2012) 880–893. doi:10.1093/treephys/tps054.

[69] M. A. El-Sharkawy, Physiological characteristics of cassava tolerance to prolonged drought in the tropics: implications for breeding culti-vars adapted to seasonally dry and semiarid environments, Brazil-ian Journal of Plant Physiology 19 (2007) 257–286. doi:10.1590/S1677-04202007000400003.

[70] D. Carvalho, S. Torre, D. Kraniotis, D. Almeida, E. Heuvelink, S. Carvalho, Elevated air movement enhances stomatal sensitivity to abscisic acid in leaves developed at high relative air humidity, Frontiers in Plant Science 6 (2015). doi:10.3389/fpls.2015.00383.

[71] W. V. Hutcheon, R. W. Smith, E. J. A. Asomaning, Effect of Irrigation on Yield and Physiological Behavior of Mature Amelonado Cocoa in Ghana, Tropical Agriculture 50 (1973) 261–272.

[72] L. Gateau-Rey, E. V. Tanner, B. Rapidel, J. P. Marelli, S. Royaert, Climate change could threaten cocoa production: Effects of 2015-16 El Niño-related drought on cocoa agroforests in Bahia, Brazil, PLoS ONE 13 (2018) 1–17. doi:10.1371/journal.pone.0200454.

[73] J. C. Suárez, F. Casanoves, M. A. N. Bieng, L. M. Melgarejo, J. A. Di Rienzo, C. Armas, Prediction model for sap flow in cacao trees under different radiation intensities in the western Colombian Amazon, Scientific Reports 11 (2021) 1–14. URL: https://doi.org/10.1038/s41598-021-89876-z. doi:10.1038/s41598-021-89876-z.

[74] J. C. S. Salazar, L. M. Melgarejo, F. Casanoves, J. A. Di Rienzo, F. M. DaMatta, C. Armas, Photosynthesis limitations in cacao leaves under different agroforestry systems in the Colombian Amazon, PLoS ONE 13 (2018) 1–13. doi:10.1371/journal.pone.0206149.

[75] M. E. McCully, C. X. Huang, L. E. Ling, Daily embolism and refilling of xylem vessels in the roots of field-grown maize, New Phytologist 138 (1998) 327–342. doi:10.1046/j.1469-8137.1998.00101.x.

[76] H. J. Schenk, S. Jansen, T. Hölttä, Positive pressure in xylem and its role in hydraulic function, New Phytologist 230 (2021) 27–45. doi:10.1111/nph.17085.

[77] H. Gouin, The watering of tall trees - Embolization and recovery, Journal of Theoretical Biology 369 (2015) 42–50. doi:10.1016/j.jtbi.2015.01.009.

[78] J. C. Motamayor, A. M. Risterucci, P. A. Lopez, C. F. Ortiz, A. Moreno, C. Lanaud, Cacao domestication I: The origin of the cacao cultivated by the Mayas, Heredity (2002). doi:10.1038/sj.hdy.6800156.

[79] E. Avila-Lovera, I. Coronel, R. Jaimez, R. Urich, G. Pereyra, O. Araque, I. Chacón, W. Tezara, Ecophysiological traits of adult trees of criollo cocoa cultivars (theobroma cacao l.) from a germplasm bank in venezuela, Experimental Agriculture 52 (2016) 137–153. doi:10.1017/S0014479714000593.

[80] FAOSTAT, FAOSTAT: Statistical database., 2019.

[81] P. Vaast, E. Somarriba, Trade-offs between crop intensification and ecosystem services: the role of agroforestry in cocoa cultivation, Agroforestry Systems 88 (2014) 947–956. doi:10.1007/s10457-014-9762-x.

[82] W. Niether, U. Schneidewind, L. Armengot, N. Adamtey, M. Schneider, G. Gerold, Spatial-temporal soil moisture dynamics under different cocoa production systems, Catena 158 (2017) 340–349. doi:10.1016/j.catena.2017.07.011.